Temporal and spatial coherence of sound at 250 Hz and 1659 km in the Pacific Ocean: Demonstrating internal waves and deterministic effects explain observations

John L. Spiesberger
Department of Earth and Environmental Science, University of Pennsylvania, 240 South 33rd Street, Philadelphia, Pennsylvania 19104-6316

(Received 16 September 2008; revised 21 April 2009; accepted 21 April 2009)

The hypothesis tested is that internal gravity waves explain temporal and spatial coherences of sound at 1659 km in the Pacific Ocean for a signal at 250 Hz and a pulse resolution of 0.02 s. From data collected with a towed array, the measured probability that coherence time is 1.8 min or longer is 0.8. Using a parabolic approximation for the acoustic wave equation with sound speeds fluctuating from internal waves, a Monte-Carlo model yields coherence time of 1.8 min or more with probability of 0.9. For spatial coherence, two subsections of the array are compared that are separated by 142 and 370 m in directions perpendicular and parallel to the geodesic, respectively. Measured coherence is 0.54. This is statistically consistent with the modeled 95% confidence interval of [0.52, 0.76]. The difference of 370 m parallel to the section causes spatial coherence to degrade deterministically by a larger amount than the effect of internal waves acting on the 142 m separation perpendicular to the section. The models are run without any tuning with data. © *2009 Acoustical Society of America.* [DOI: 10.1121/1.3133243]

PACS number(s): 43.30.Re [RCG] Pages: 70–79

I. INTRODUCTION

The temporal and spatial coherences of sound are estimated from a towed receiving-array with signals originating from an acoustic source over the Hoke seamount at 1659 km distance [Fig. 1(e)]. The signal is centered at 250 Hz with a bandwidth of 50 Hz (1/50=0.02 s pulse resolution). We test the hypothesis that coherence scales are accurately modeled by fluctuations of internal gravity waves obeying the Garrett–Munk spectrum.[1,2] The test uses standard methods in acoustics and oceanography with no effort to tune the models with data. A Monte-Carlo technique yields time-varying impulse responses at the receiver by evolving the internal wave field using a linear dispersion relation. If the temporal scales from the data and model agree, it would be the fourth time agreement is found using the models in this paper (Table I, Fig. 1). Another comparison with data is inconclusive because acceleration of the instruments is not accounted for even though it appears that acceleration significantly affects coherence.[6] If the spatial scales of coherence from the towed array are consistent with measurements, it would also be the fourth time that the standard spectrum for internal waves could account for such phenomena.[7–10] One of these analyses uses the data to set a model parameter to fit the data.[9] It appears that model does not compare well without tuning with data.

There are two reasons for again testing the ability of models to predict coherence. First, coherence is important for acoustic communication, signal processing, acoustical oceanography, and theoretical studies. Second, the author does not believe enough comparisons with data have been made for enough frequencies, distances, and oceans to state with certainty when modeled coherence yields accurate predictions. It appears justifiable to form a strong scientific background comprised of hundreds of papers published by numerous investigators. In this paper, comparison of temporal coherence is made at higher frequency and shorter distance than before. Previous frequencies were near 75 and 133 Hz,[3–5] and involved distances between 3000 and 4000 km.

II. EXPERIMENT AND DATA PROCESSING

A Hydroacoustics HLF-5 source was deployed over the Hoke seamount in the North Pacific in 1999 by Chiu and co-workers.[11,12] It was located at 32.105 33° N 233.088 83° E at a depth of 673 m. It is tautly moored 104 m above its anchored position on the seamount. We concern ourselves with a single transmission at 00:00 Greenwich Mean Time on 14 September, 1999. The transmission consists of 11 periodic linear shift register *M*-sequences lasting 135.036 s. Each period lasts 12.276 s and consists of 1023 digits. Each digit consists of three cycles of carrier at 250 Hz, and is encoded by modulating the phase of the carrier by $\pm 88.209\ 22°$. The sequence law is 2033_8. The source level is 192 dB re 1 μPa at 1 m (132 W). The pulse resolution is about 0.02 s. Bathymetry of the Hoke Seamount was measured using a Knudsen echo-sounder from the R/V POINT SUR in May 1999.[11]

The signal was received on a towed array at 171 m depth near 46.9023° N and 230.3542° E. The location is written with greater precision than its accuracy of 1 km so that others can reproduce the model results of this paper. The ship was heading at 12° true at a speed of about 1.7 m/s. Since the bearing angle from the source is about −9° true, the signal arrives near endfire [Fig. 1(e)]. Data were separately processed from two parts of the array to investigate spatial coherence. Going perpendicular to the geodesic between the source and receiver, the ends were separated by 142 m. In a

 0001-4966/2009/126(1)/70/10/$25.00

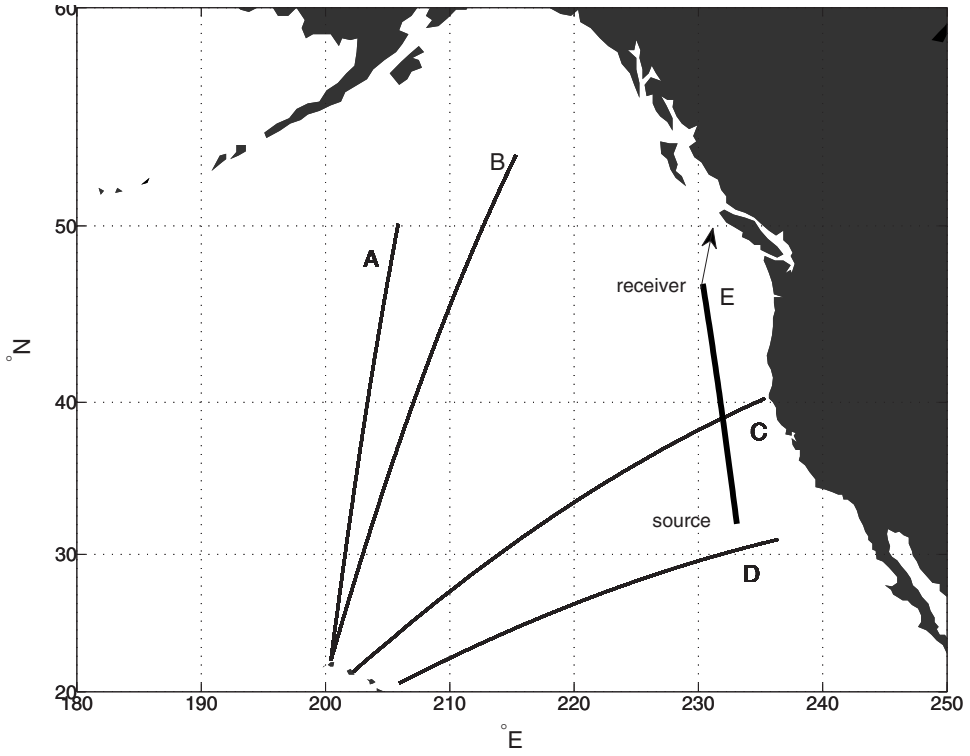

FIG. 1. Five sections where blind predictions of coherence time have been made. (A) 3115 km between a bottom-mounted source on Kauai (75 Hz, 0.03 s resolution) and a towed receiver, (B) 3683 km between the same source and a towed receiver, (C) 3709 km between a bottom-mounted source at Kaneohe Bay, Oahu (133 Hz, 0.06 s resolution) to SOSUS station mounted on the bottom, (D) 3250 km transmission between source dangled from R/V Flip (75 Hz, 0.03 s resolution) and a vertical array, and (E) 1659.32 km transmission reported in this paper between a source moored over the Hoke seamount (250 Hz, 0.02 s resolution) and a towed array. Heading of the towed array is 12° true (arrow).

direction parallel to the geodesic, the ends are separated by 370 m. These are called the "cross" and "along" geodesic separations, respectively.

A beam is steered toward the source from each end using a standard non-adaptive time-domain beamformer. The beam is much wider than any variation in signal direction. Data are Doppler corrected for each separate M-sequence period to yield the largest output of a matched filter. The signal-to-noise ratio (SNR) of the highest peak in each period was about 29 dB. In this paper, the level of noise used in computing the SNR is computed from a portion of the impulse response where signal does not occur. Using the best Doppler correction for each period, a coherent average was applied to 9 of the 11 periods, yielding a peak SNR of 38 dB [Fig. 2(a)]. 2 of the 11 periods were unprocessed to avoid end-effect sidelobes that occur when match filtering with an M-sequence.[1] Coherence times up to nine periods, or $12.276 \times 9 = 110.484$ s, can be investigated here. The ship traveled $1.7\ \mathrm{m/s} \times 110.484 = 188$ m during this interval.

TABLE I. Summary of five experiments where a Monte-Carlo technique is used to see if modeled and measured coherence times of sound are consistent. Section letter refers to Fig. 1. Analysis of sections A, B, and C are from Refs. 3–5, respectively. Results from section D are inconclusive because observations of coherence time may not quite be complete (Ref. 6). This paper concerns section E.

Section	Distance (km)	Frequency (Hz)	Pulse resolution (s)	Data-model agree?
A	3115	75	0.03	Yes
B	3683	75	0.03	Yes
C	3709	133	0.06	Yes
D	3250	75	0.03	Inconclusive
E	1659	250	0.02	Yes

Coherent averages are constructed by weighting records according to their noise variance. The result for complex demodulate d_i is

$$\overline{d}_i(J) = \frac{\sum_{j=1}^{J} d_i/\sigma_j^2}{\sum_{j=1}^{J} 1/\sigma_j^2}, \tag{1}$$

where J is the number of coherent averages, and the variance of the noise in record j is σ_j^2. The variance of the noise is estimated from a portion of the impulse response without signal.

Because location of the array is only known within 1 km, it is not possible to compare with models the absolute time of signal propagation between the source and receiver.

III. MODELS

Models for the oceanic environment and the propagation of sound are described next.

A. Environment

As there were no *in-situ* environmental measurements, climatological archives of ocean properties were used in the modeling. They are almost always sufficiently accurate to derive an acoustic impulse response that looks like day-long averages of the measured response.[13] The speed of sound along the section is computed with Del Grosso's algorithm[14] and Levitus' climatological averages[15] of temperature and salinity for summer. The depth of minimum speed varies from 560 m at the source to 430 m at the receiver. Since the acoustic models use Cartesian coordinates, the sound-speed profiles are translated to Cartesian coordinates using the Earth-flattening transformation.[16]

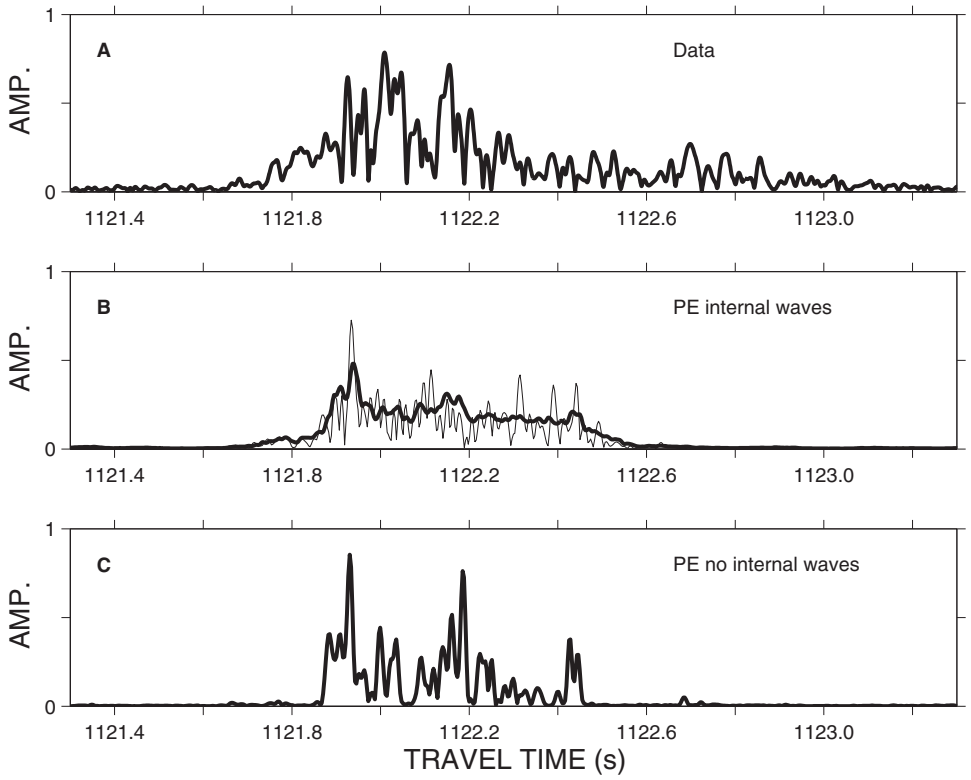

FIG. 2. Coherent average of impulse response from Hoke source (A) compared with two models [(B) and (C)]. Travel time of the data is adjusted to approximately coincide with the models. Only panels (B) and (C) have amplitudes that can be compared. PE is the parabolic approximation. Panel (B) shows an incoherent average (thick line) from many realizations of the impulse response computed at different geophysical times through an evolving field of internal waves. The thin line shows one of those realizations. Panel (C) is the impulse response computed through a climatological average of sound speed without perturbations from internal waves.

Internal waves are modeled with the Garrett–Munk[1,2] spectrum, with details published elsewhere.[17] Currents are ignored, being two orders of magnitude less than sound-speed perturbations arising from adiabatic vertical displacements of water in the upper ocean. The perturbations are added to the climatology of sound speed described above. The complete set of internal wave modes is precomputed and retrieved as needed at range intervals of 80 km to account for changes in water depth, buoyancy frequency, and sound speed. Vertical displacements of these modes are set to zero at the surface and bottom. For each 80-km interval, a three-dimensional field of internal waves is computed in a box of 80 km $\times$ 80 km $\times D$ m where D is the average depth of the ocean in that interval. A vertical slice through the box gives the vertical displacements along the geodesic for any desired section. Temporal evolution of the field is governed using the linear dispersion relation. The energy of the internal wave field is taken to be that specified by Garrett and Munk.[1,2]

Bathymetry along the section consists of a steeply sloping region at the seamount, followed by an abyssal region until 900 km (Fig. 3). This is followed by a region marked by ridges and seamounts over a bottom with depths between 2500 and 3000 m. Older and newer bathymetric databases are shown to indicate substantial differences (Fig. 3). Although the model uses the newest data, it is not clear if it is accurate enough to yield an accurate impulse response of the acoustic field.

The parabolic approximation of the acoustic wave equation requires parameters to describe acoustic propagation in the bottom of the ocean. These are provided to make it easier for others to replicate our model. The thickness of the sediment, and the ratio of the sediment to water density are taken from the Laske-Masters database at 50-km intervals.[18] The thickness varies non-monotonically along the section within the interval 155–407 m. The thickest sediments occur at distances between 550 and 1300 km from the source. The sound speed at the top of the sediment divided by that at the bottom of the water column is 1.02. The density of the sediment varies from 1.8 to 1.7 gm cm^{-3}. The attenuation in the sediment is

$$\alpha(f) = \alpha_0 f^p \quad (\text{dB m}^{-1}), \tag{2}$$

where f is the frequency in kHz, $p=1$, and $\alpha_0 = 0.02$ dB m^{-1} kHz^{-1}. The speed in the sediment is taken to increase with depth as 1 s^{-1}. The speed in the basement divided by that at the bottom of the sediment layer is 2. The density of the basement layer is 2.5 gm cm^{-3}. The attenuation in the basement is given by Eq. (2) except $\alpha_0 = 0.5$ dB m^{-1} kHz^{-1} and $p=0.1$. While all these geoacoustic parameters may not match those along the section, coherence of modeled multipath is probably insensitive to their values. They would likely change their amplitudes, but this does not seem to be important for comparing measured and modeled probability distributions of coherence in time nor modeled values of spatial coherence as long as most observed paths are present in the model.

B. Acoustic models

This parabolic approximation[21] outputs a two-dimensional field of sound along the geodesic from 0- to 8000-m depth. Tests suggest that travel times of pulses are computed with an accuracy of a few milliseconds.[21] The result is insensitive to reasonable variations in a reference speed of sound, which is why it is called the sound-speed insensitive approximation. The impulse response is com-

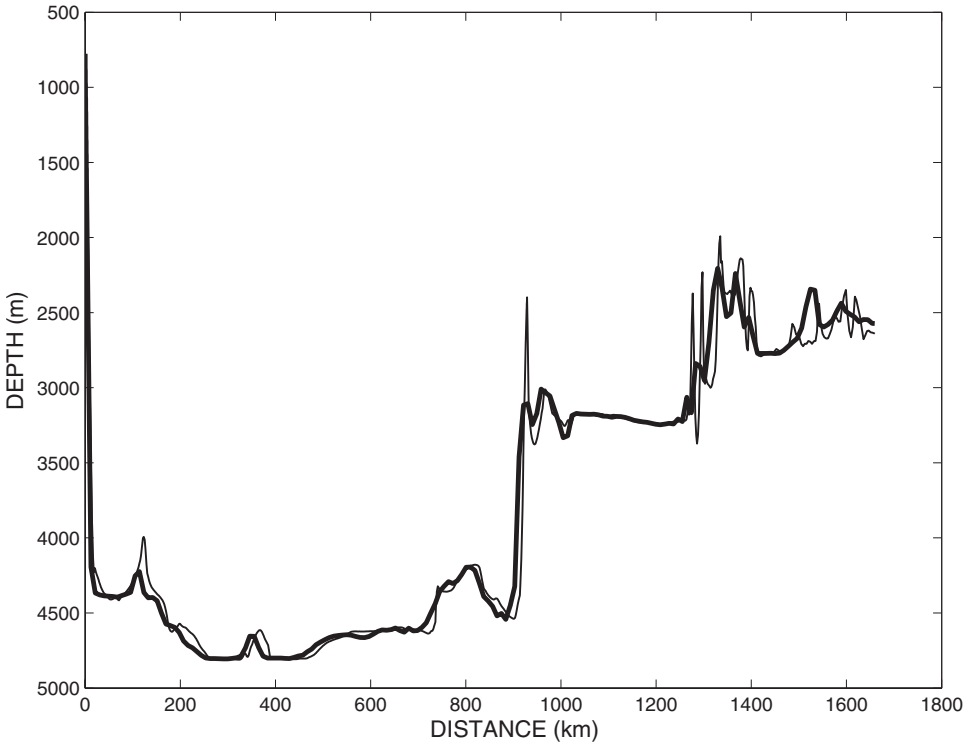

FIG. 3. Two estimates of bathymetry along section E in Fig. 1. Both estimates incorporate experimental measurements of bathymetry within 2.8 km of the acoustic source moored over the Hoke seamount (Ref. 11). The thicker line is from a 1987 database of depth (Ref. 19). The thinner is from a 2006 database (Ref. 20).

puted by applying an inverse Fourier transform to many single-frequency computations. Calculations of horizontal coherence of sound at the receiver are made assuming sound propagates without effects due to diffraction, refraction, and scattering in the horizontal coordinate. Instead, computations are made by approximating the solution of the acoustic wave equation with two-dimensional vertical slices through the modeled ocean. Despite the ubiquitous use of this vertical slice approximation, a rigorous justification has apparently not been published for the frequency considered here (250 Hz). Vertical slices of sound speed are obtained from the three-dimensional field of internal waves (Sec. III A). The convergence of the parabolic approximation is found by halving the grid sizes until the answers do not change significantly. We use a vertical grid spacing of 1.95 m. The grid separation in the horizontal dimension varies between 10 and 50 m. A separation of 10 m is used when the bathymetry is steep, such as near the Hoke seamount.

IV. IMPULSE RESPONSE

The SNR increases monotonically with the number of M-sequence periods coherently averaged. As mentioned in Sec. II, the peak SNR from each processed period is 29 dB. If each period was perfectly coherent and the noise was uncorrelated from period-to-period, a coherent average of all nine periods would have a SNR of $29+10\log_{10}9=38.5$ dB. This is about the same as the 38 dB measured from the coherent average [Fig. 2(a)]. The coherent averaging scheme that uses variable Doppler for each M-sequence period appears to yield a SNR close to the best that can be expected from theory.

The impulse response starts near 1121.75 s and ends near 1123.5 s [Fig. 2(a)]. This is aligned by eye to the best model result available in this paper [Fig. 2(b), thick line]. [Comparison of absolute times is impossible because location of the receiver is uncertain within 1 km (Sec. II).] This model is an incoherent average of 61 impulse responses computed through internal waves at 3-h intervals. Each impulse response is synthesized from 512 single-frequency runs of the parabolic approximation.[21] We find that separate incoherent averages from the first 31 and last 30 impulse responses are similar (not shown). Therefore, the incoherent average converged. 1 of the 61 impulse responses is shown [Fig. 2(b), thin line] to give an idea of how much the incoherent average smoothes a typical impulse response. Note the energy lasts longer in the data than the model by about 1 s [Fig. 2(a)]. This could be due to errors in bathymetry or too much attenuation in the bottom for later-arriving multipath. Another possibility is that the acoustic energy undergoes an extension in time due to a bias incurred from oceanic mesoscale. This hypothesis has been discussed, but not confirmed definitely.[17] Our environmental models do not include a mesoscale. The author believes it unlikely that uncertainty of energy in the internal wave spectrum would lead to an extension of 1 s, but this possibility cannot be excluded with certainty without further modeling. This is beyond the scope of this paper.

Without internal waves, the impulse response is shorter [Fig. 2(c)]. One may question why the jagged nature of the measured impulse response seems to better resemble the model in panel (C), without internal waves, than the thick line in panel (B), which includes internal waves. The reason is due to the smoothing of the impulse response that created the thick line in panel (B) through its incoherent averaging of 61 separate impulse responses. A single modeled impulse response through internal waves is usually less smooth [thin line, panel (B)]. The model in panel (C) is not an average, and neither is the measurement in (A). From past

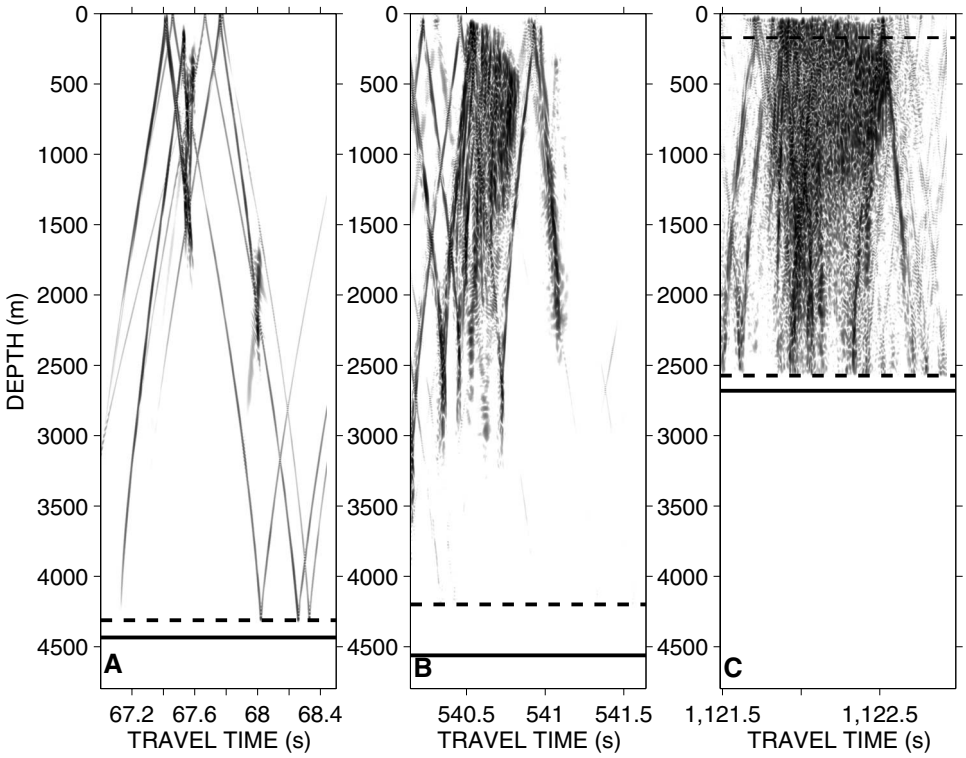

FIG. 4. Time fronts at distances of 100, 800, and 1659 km from source in panels (A), (B), and (C), respectively. Levels shown are in upper 38 dB at each distance. Depths of the water and basement are dashed and solid lines, respectively. Each panel shows 1.5 s of acoustic travel time. Top dashed line in panel (C) is at depth of the receiver. Time fronts are modeled with the parabolic approximation (Ref. 21) for a snapshot of sound-speed fluctuations due to internal waves added to a climatological background.

experience,[13] we believe that a daily or longer incoherent average of measured impulse responses would better resemble the thick line in panel (B) than in panel (C).

A. Interactions with surface and bottom

Time fronts indicate that the signal interacts with the surface and bottom of the ocean (Fig. 4). The top 38 dB are shown at each range because this is the SNR in the impulse response derived from the coherent average [Fig. 2(a)]. At distances exceeding about 1000 km, interactions with the surface appear to occur more frequently (not shown) because the acoustic waveguide rises toward the surface in the northern cold water. Reports from NOAA/NODC buoys and the volunteer ship observing program indicate crest to trough wave heights between 3 and 4 m along this section on 14 September 1999. The standard deviation of wave height is about 1 m.

The Rayleigh parameter, $P \equiv 2kh \sin\theta$, is useful for estimating effects of surface waves on sound, where the acoustic wavenumber is k, rms displacement of the surface is h, and grazing angle of sound with respect to the surface is θ.[22] For the center frequency of 250 Hz, and a rather large grazing angle of 5°, $P \sim 0.17$. This extreme case is much larger than predicted from ray traces (not shown), so the actual values for P would be less. For P much less than 1, the scattered wave can be thought of as specularly reflecting from the surface with rms variation of radian acoustic phase given by P.[22] The calculation is a ray approximation where the distance of a path is modified by a single interaction with the rough surface. At finite frequency and finite bandwidth, the region that influences each multipath expands from a point to a finite horizontal region. The region expands with decreasing frequency and increasing distance of transmission.[23] For example, at 2500 Hz and a transmission distance of 600 km, the region of influence is about 10 km (Fig. 9 in Ref. 23). The region would be larger in this experiment. We approximate the net effect of sound interacting with the rough surface over one 10-km region as follows. Since a typical crest-to-crest distance is about 50 m, there are $n \equiv 10\,000/50 = 200$ waves that interact with sound in 10 km. This reduces the rms value of P for a single wave by the factor $1/\sqrt{n}$. The rms phase variation of 0.17 rad for one interaction is reduced to $0.17/\sqrt{200} = 0.012$ rad. At 1659 km range, and an acoustic interaction with the surface every 50 km, there are at most $1659/50 \sim 33$ encounters of sound with the surface. At 50-km spacings, the net effect of phase with each surface interaction is statistically independent. Therefore, the net rms phase from 50 interactions is a random-walk process that increases by $\sqrt{33}$ the rms phase change from 0.012 to $0.012\sqrt{33} = 0.07$ rad. This is a negligible variation in multipath phase at the receiver. Effects of surface waves are too small to affect measurements of coherence.

Bottom spectra are less well known than the spectrum of surface waves. However, it does not appear that acoustic interaction with the bottom during the 135-s long transmission affects arrival structure. For the transmission, the ship moves 370 m away from the source (Sec. II). The scale of influence for the bottom is probably similar to that for the surface, i.e., 10 km or more. Since $370/10\,000 \ll 1$, it seems unlikely that the bottom significantly affects coherence.

V. TEMPORAL CORRELATION

In Sec. IV, we found that all nine impulse responses could be coherently averaged to increase the SNR over that for any individual impulse response. In this section, we increase the degrees of freedom by computing coherence time in small time windows from each impulse response.

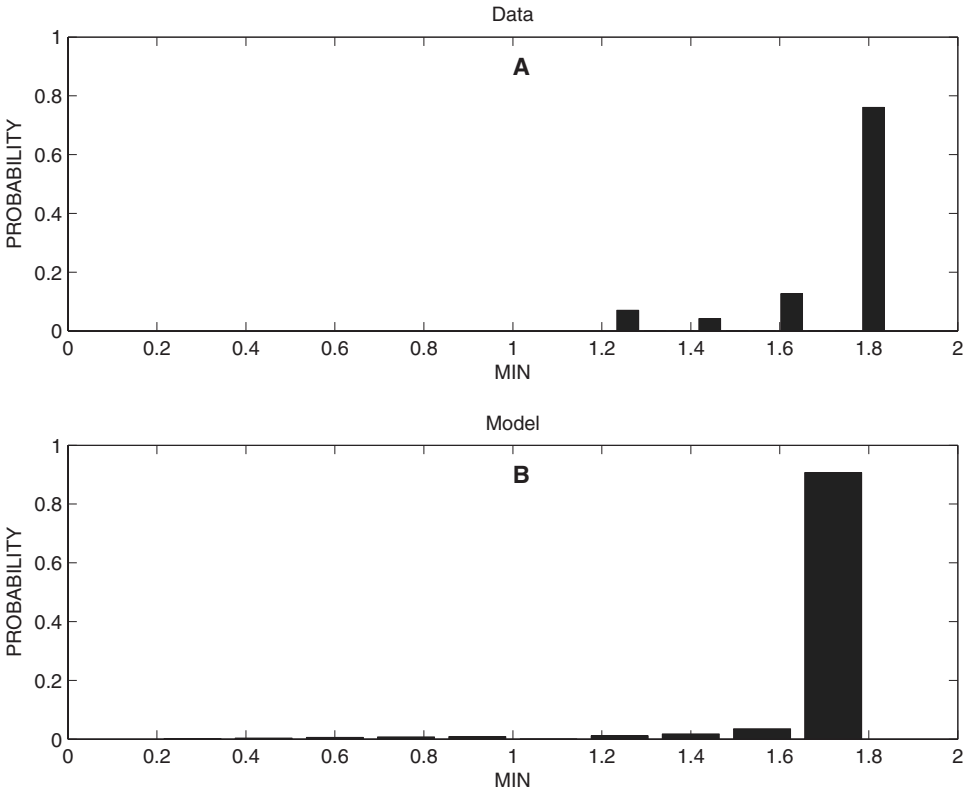

FIG. 5. Probability distribution of coherence time from section E (Fig. 1) for the data (A) and model (B). Data come from a single transmission of the Hoke source covering 1.833 min. Coherence time of the data is discretized to 12.276 s, the period of each of the nine transmitted M-sequences. Coherence time of the model is discretized at 12 s intervals. Coherence times from data and model are analyzed on the same basis. Actual coherence times may extend past 1.833 min, but cannot be explored with a transmission of 1.833 min. The sum of the probabilities is one for each panel separately.

A. Data

Data are Doppler corrected as described in Sec. II. The resulting impulse response for each of 9 periods is subdivided into 71 windows of travel time of duration 0.02 s each. The windows are chosen to cover energetic arrivals lasting 1.42 s. Even though the peak SNR of the entire impulse response increases monotonically with the number of added M-sequence periods (Sec. IV), this is not necessarily what happens when subsections of the impulse response are considered separately. For each window, we compute the peak SNR for each coherent average via Eq. (1) starting from periods 1 to 9. Letting m denote the period yielding maximum SNR, coherence time for that window is computed using $T=m12.276/60$ min. An empirical probability distribution is plotted for these 71 values [Fig. 5(a)]. The most likely coherence time is 1.8 min. It occurs with probability 0.8. Lesser coherence times are distributed between 1.2 and 1.6 min. The probability distribution is insensitive to modest changes in window duration. For example, when the duration is changed from 0.02 to 0.05 s, the distribution looks almost the same (not shown).

We now turn to the question as to whether the observed variation of 0.1 m/s of effective Doppler during 1.8 min is caused by the ocean or the instruments. Our previous experience with tautly moored sources in the Pacific and Atlantic is consistent with maximum speed, v_0, of a few cm/s near semi-diurnal and diurnal periods. Therefore, change in source speed in geophysical time interval τ has maximum value, $\delta v=2\pi\tau v_0/T$, where T is the period. For $v_0=0.02$ m/s, $\tau=1.8$ min, and $T=12$ h, $\delta v=3.1\times10^{-4}$ m/s. This is too small to explain a 0.1 m/s change in Doppler. On the other hand, a change in 0.1 m/s is entirely possible for the towed receiver. Changes in barotropic currents or other short-term fluctuations of currents and sound speeds, including internal waves following a Garrett–Munk spectrum, are more than a factor of 10 too small to account for the observed Doppler change of 0.1 m/s (Sec. VA of Ref. 4). Acceleration of the receiver is the only mechanism we can think of that could cause the observed variation in Doppler. It is likely that the variable Doppler correction merely removes effects from receiver acceleration and does not contaminate the measured estimates of coherence time.

B. Model

The parabolic approximation yields the impulse response for 122 records at 12 s intervals. (Internal waves evolve by 12 s between computations.) This allows a comparison of coherence time near the same resolution as the data (12.276 s).

The impulse response of each record is subdivided into $W\equiv41$ adjacent windows of width 0.02 s. This covers the modeled impulse response lasting 0.8 s [Fig. 2(b)]. White Gaussian noise with mean zero and variance σ^2 is added to each record. The SNR of each realization is set to be the same as the data in the following sense. Let the peak amplitude of record j be $\hat{a}_j$, $j=1,2,3,\ldots,122$. The record-averaged peak amplitude is $\bar{a}=122^{-1}\Sigma_{j=1}^{122}\hat{a}_j$. The variance is determined by solving for σ^2 in $29=10\log_{10}(\bar{a}^2/\sigma^2)$ (dB). This ensures that the record-average peak SNR is the same as measured.

A bootstrap scheme is used to estimate coherence time for each of 41 windows. First, we select at random $B=3000$ different starting records among 122 possibilities. The direction of the coherent average is selected at random to go forward or backward in time with respect to the starting

record. Nine total records are added together in the randomly chosen direction. End point problems are handled by choosing a direction that would not extend below 1 or above 122. With nine records, we are exploring coherence times up to 9 records $\times$ 12 s/record/(60 s/min) = 1.8 min. For each starting record, coherence time is computed by selecting the number of records, n, yielding the largest SNR where n can go from 1 to 9. The coherence time is $12n/60$ min. Letting coherence time for bootstrap b of travel time window k be T_{bk}, there are $BW = 3000 \times 41 = 123\,000$ estimates of T_{bk}. An empirical probability distribution is computed from these [Fig. 5(b)]. It is similar to the data. The most likely coherence time is 1.8 min, occurring with a probability of 0.9. Histogram-bars have slightly different centers for the model and data because the data and model are available at 12.276 and 12 s intervals, respectively.

VI. SPATIAL CORRELATION

A. Data

Coherent averages from 9 M-sequence periods were computed from two sub-arrays whose cross- and along-geodesic separations are 142 and 370 m, respectively (Sec. II). Each coherent average is computed by beamforming, using a matched filter with the emitted waveform, and by using a variable Doppler scheme for each period to optimize average SNR. The peak SNR of each coherent average is 38 dB. The energetic portion of each coherent average is about 1.5 s. A normalized cross-correlation coefficient is computed between the single coherent average from one array with the single coherent average from the other array. The value of the correlation coefficient is 0.54. The SNR is so high that virtually none of this degradation in coherence is explained by noise.

B. Models

Degradation of spatial coherence in the presence of internal waves is computed using our model that places a horizontal array at fixed distance from the acoustic source. In other words, it does not have the flexibility of letting the array be anything except perpendicular to the geodesic between source and receiver. The array is, however, not perpendicular to the geodesic. For convenience, we therefore divide the modeling of spatial coherence into effects due to cross-geodesic and along-geodesic components. Dividing analysis into two components allows identification for independent causes for de-coherence.

1. Cross-geodesic separations

We estimate the extent to which a horizontal separation of 142 m (perpendicular to the section) can explain the measured correlation coefficient of 0.54. At 1659 km distance, a 10-km horizontal array is placed perpendicular to the geodesic with elements at 10 m spacing. Vertical sections of sound speed are taken from the three-dimensional field of internal waves between the source and each element on the array. No attempt is made to model effects due to horizontal coupling between the vertical sections. A similar approach has been discussed elsewhere.[7] The approximation has only been shown to be valid up to a frequency of 75 Hz.[24] It might be valid at higher frequencies, but a direct numerical confirmation apparently awaits future investigation.

The acoustic field at 250 Hz only is computed at each array element for eight geophysical times at 8.4 h intervals. An 8.4 h interval is more than enough to yield uncorrelated impulse responses for this model. Using the bootstrap, we find the normalized correlation coefficient for cross-geodesic separation falls to e^{-1} at 0.5 km (Fig. 6). Note the tight bounds on correlation coefficients at the 95% confidence limit. Since there are eight uncorrelated realizations of the acoustic field on a 10-km long array, there are about $8 \times 10/0.5 = 160$ degrees of freedom. Reading from the figure, we see that the correlation coefficient is between 0.904 and 0.918 at 142 m. We conclude that a cross-geodesic separation of 142 m cannot explain the measured correlation coefficient of 0.54. We will see next that another mechanism does explain a coefficient of 0.54 when combined with the values between 0.904 and 0.918 here.

2. Along-geodesic separation

We estimate coherence of the signal between two points on the geodesic separated by 370 m. The parabolic approximation is used to compute the impulse response through the same fluctuating internal wave field as before [Fig. 7(a)], except the final range is decreased by 370 m. Comparing 61 impulse responses separated by 370 m at 3-h intervals, the mean and standard deviation of the normalized cross-correlation coefficient are 0.73 ± 0.079. The 95% confidence limits are in the interval [0.57, 0.83]. The lower limit is close to the measured value of 0.54.

There appear to be three hypotheses for degradation of modeled coherence in the along-geodesic component. (1) Acoustic signals are affected by different components of the internal wave field. (2) Travel times of multipath are sensitive to interactions of sound with bathymetric features in the presence of internal wave fluctuations. (3) The travel time change for energy arriving at different inclination angles is differentially affected for along-geodesic displacements in the absence of internal waves. The first hypothesis does not explain the degradation because we compute about the same degradation when internal waves are absent. The second hypothesis does not explain the degradation because we obtain the same answer when the bathymetry is changed to be flat at 5 km of depth. The third hypothesis does appear to explain the degradation. Using realistic bathymetry, but not internal waves, the computed correlation coefficient is 0.7. This value is within one standard deviation of the correlation coefficient computed with internal wave fluctuations reported above (i.e., 0.73 ± 0.079).

An analytical calculation seems to confirm that degradation of correlation is primarily explained by the third hypothesis. The change in acoustic phase for ray i at frequency f due to a receiver horizontally displaced by δx along a geodesic is

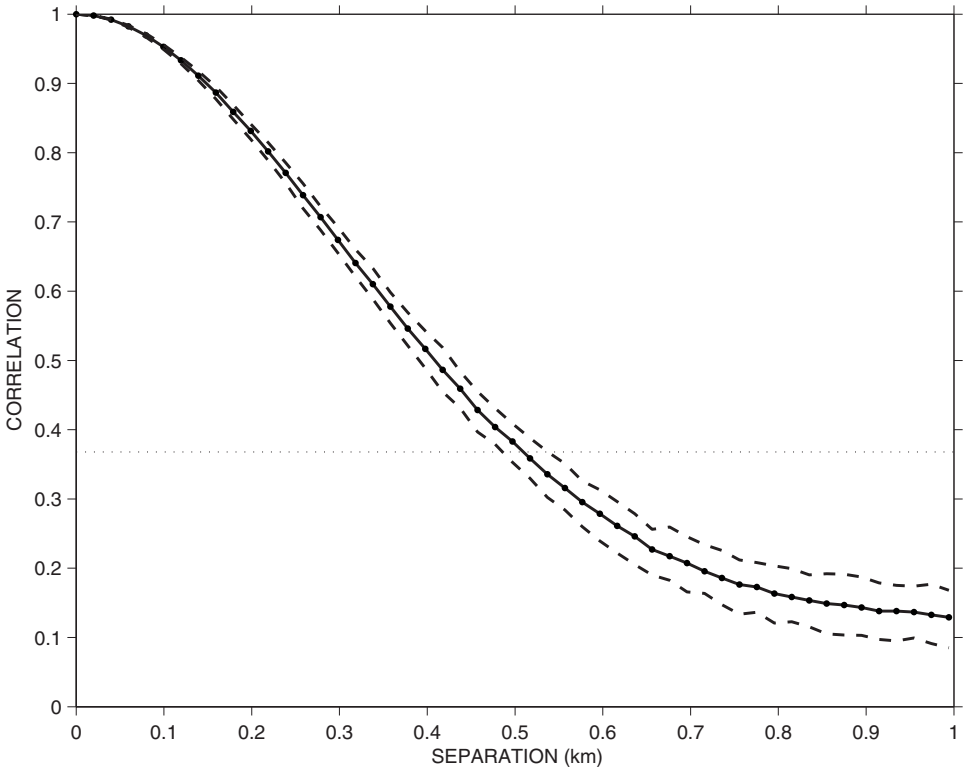

FIG. 6. Modeled estimates of the normalized horizontal correlation coefficient of the acoustic field for section E in Fig. 1 at 250 Hz with 95% confidence limits shown. The dotted line is at exp(−1). The correlation decreases with separation because of the effects of internal gravity waves.

$$\delta\phi_i \approx \delta x f \cos\,\theta_i/c \quad \text{(cycles)}, \tag{3}$$

where θ_i is the inclination angle of the ray at the receiver, measured positive up from the horizontal. The equivalent change in travel time is $\delta t_i = \delta\phi_i/f$. The result is based on the linearized assumption that the ray angle does not change significantly for horizontal displacement δx. Consider I temporally-resolved arrivals with amplitudes a_i, $i = 1,2,3,\ldots,I$ that have a simple time series

$$b(t) = \sum_{i=1}^{I} a_i \cos[\omega(t - T_i)]\Pi\left[\frac{t - T_i}{3\Delta/2}\right], \tag{4}$$

where the boxcar function, Π, equals unity when its argument has absolute value of 1 or less, and is 0 otherwise. The travel time of ray i is T_i, the period of the sinusoid is $\Delta = 2\pi/\omega$, and the speed of sound at the receiver is c. The boxcar is unity for three periods, which is the same as the emitted signal for this experiment. Thus, each arrival is represented by three cycles of carrier. When the receiver is moved by δx along the geodesic, the predicted time series is

$$q(t) = \sum_{i=1}^{I} a_i \cos[\omega(t - T_i - \delta t_i)]\Pi\left[\frac{t - T_i - \delta t_i}{3\Delta/2}\right], \tag{5}$$

assuming a_i are unchanged. To calculate the maximum value of the cross-correlation coefficient between $b(t)$ and $q(t)$, we approximate the maximum lag to occur at δt_1. We further assume that the cross-correlation coefficient is primarily degraded due to changes in phase between corresponding paths once corresponding paths in $b(t)$ and $q(t)$ are approximately lined up at lag δt_1. This approximation neglects degradation due to the fact that the boxcar envelopes for corresponding paths will not quite line up due to differential effects of travel time caused by various values of θ_i. Noting that the time-mean values of $b(t)$ and $q(t)$ are zero, the normalized correlation coefficient has maximum value

$$\rho = K/J, \tag{6}$$

where

$$J = \int b^2(t)dt = \int q^2(t)dt = \sum_{i=1}^{I} a_i^2 \int_{-3\Delta/2}^{3\Delta/2} \cos^2\frac{2\pi t}{\Delta}dt$$

and

$$K = \int b(t)q(t + \delta t_1)dt.$$

Then,

$$K \approx \sum_{i=1}^{I} a_i^2 \cos(\delta\phi_i - \delta\phi_1) \int_{-3\Delta/2}^{3\Delta/2} \cos^2(\omega t)dt.$$

Substituting K and J into ρ we get

$$\rho \approx \frac{\sum_{i=1}^{I} a_i^2 \cos[\delta x f(\cos\,\theta_i - \cos\,\theta_1)/c]}{\sum_{i=1}^{I} a_i^2}. \tag{7}$$

For the simple case of $a_i = 1$,

$$\rho \approx \frac{1}{I}\sum_{i=1}^{I} \cos[\delta x f(\cos\,\theta_i - \cos\,\theta_1)/c] \quad \text{for } a_i = 1, \tag{8}$$

so all the degradation is due to differences in arrival angle. For the simple case of two arrivals, we solve for δx

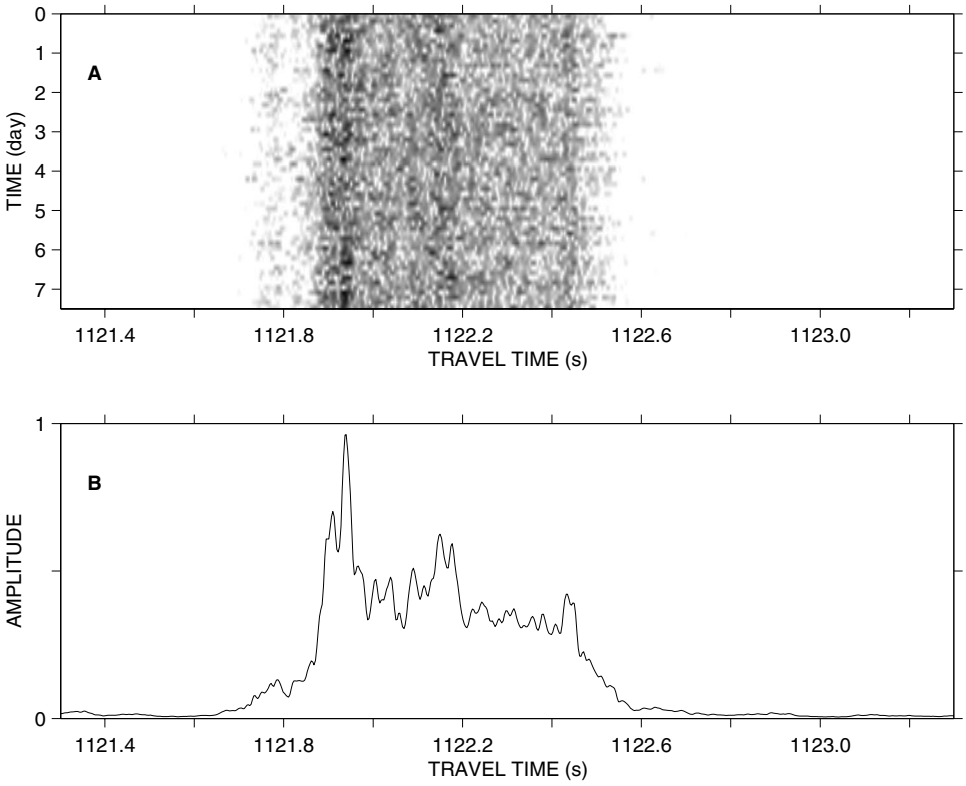

FIG. 7. (A) Contours of top 30 dB of 61 impulse responses, at 3-h intervals, computed from the parabolic approximation model for section E in Fig. 1. Modeled variations are due to the time evolution of a standard internal wave field. (B) Incoherent average of the 61 impulse responses used in (A) [same as thick line in Fig. 2(b) except amplitudes are scaled with a different value].

$$\delta x \approx \frac{c \cos^{-1}(2\rho - 1)}{f(\cos\ \theta_2 - \cos\ \theta_1)}. \tag{9}$$

Using a modeled value of $\rho=0.7$, and for typical arrival angles of eigenrays, $\theta_1=2°$ and $\theta_2=9°$, the needed along-geodesic displacement, δx, is 610 m. This is less than a factor of 2 from the measured displacement of 370 m and confirms this hypothesis for explaining decorrelation in the along-geodesic direction.

3. Combined along- and cross-geodesic effects

We seek 95% confidence limits for the cross-correlation coefficient due to the combined effects of along- and cross-geodesic separations. It is likely that effects from along- and cross-geodesic separations are approximately statistically independent. So, it is likely that $\rho \approx \rho_a \rho_b$ where ρ_a and ρ_b are the coefficients due to along- and cross-geodesic separations, respectively. The formal method for estimating confidence limits for ρ is to empirically draw pairs of model realizations of ρ_a and ρ_b, then form their product to obtain a realization of ρ. From these, 95% confidence limits are obtained empirically. We sidestep this procedure because the 95% confidence limits for cross-geodesic separation are narrow. We approximate $\rho_b=0.91$, its mean value at a separation of 142 (Fig. 6). Since the 95% confidence interval for ρ_a is [0.57, 0.83], we approximate the 95% interval for ρ as $0.91 \times [0.57, 0.83] = [0.52, 0.76]$. This is statistically consistent with the measured value of 0.54. We did not attempt to find a confidence limit for the measured value because only one realization of spatial coherence is available and the SNR is so high that effects from noise are negligible.

VII. CONCLUSIONS

We tested the hypothesis that the Garrett–Munk spectrum of internal gravity waves accounts for observations of temporal coherence of sound for a 1659 km section in the Pacific Ocean [Fig. 1(e)]. Sounds emanated from a 250 Hz source following a phase-coded signal with 0.02 s resolution. Without any tuning of the oceanographic or acoustic models to fit the data, we obtain similar modeled and measured probability distributions of temporal coherence.

The model for spatial coherence is statistically consistent with the measured value of 0.54. The model needs two components to yield this result. The first is the decorrelation of the signal due to internal waves due to displacements perpendicular to the section. The second is a deterministic effect due to the difference in distance between the source and two arrays at either end of the complete towed array. The array is not perpendicular to the section. In this experiment, the deterministic effect leads to a larger loss of spatial coherence than the effects from internal waves.

Modeled degradation of spatial coherence due to internal waves is computed assuming negligible interaction of sound between separate vertical slices of the acoustic field. An indirect confirmation of this approximation appears to come from the statistical consistency between measured and modeled values of spatial coherence.

Varying model parameters to test sensitivity of the results does not seem critical in predicting coherence in light of the resemblance with data using archival parameters. This paper is not a study in sensitivity analysis. It simply seeks to determine whether the models are reliable predictors of coherence, and they are. This is an important finding. Another study might investigate modifying the spectrum for internal

waves. However, variations should be done realizing the spectrum from the literature was fitted to myriads of hydrographic data collected world-wide.

It is important to continue comparing with models coherence from other experiments since coherence is important for numerous applications (Sec. I). Comparison here is made at higher frequencies and shorter ranges than before (Sec. I).

It is possible that the probability distribution for coherence time could exceed 1.8 min. We did not address this question because the hypothesis is untestable with our data. What seems to be important is that the modeled probability distribution looks like that derived from data when both are analyzed in the same way.

Finally, the Monte-Carlo impulse responses are run on a supercomputer. Others are working on faster methods for implementing Monte-Carlo methods.[25]

ACKNOWLEDGMENTS

This research was supported by the Office of Naval Research Contract No. N00014-06-C-0031 and by a grant of computer time from the DOD High Performance Computing Modernization Program at the Naval Oceanographic Office. I thank Curt Collins, Chris Miller, and Ching-Sang Chiu, of the Naval Postgraduate School, for providing bathymetry of the Hoke seamount and providing answers to my inquiries on their experiment with this source. I thank Eric Freeman (NOAA) for helping me obtain surface wave data from ships. I thank the editor, Roger Gauss, and reviewers for their valuable and detailed suggestions.

[1]We might have been able to use ten *M*-sequences to avoid sidelobes. However, the matched filter output contains sidelobes in the time domain if the replica is correlated with data containing no signal (i.e., before signal arrival and after signal termination). To be safe we analyzed nine interior *M*-sequence periods.

[1]C. Garrett and W. Munk, "Space-time scales of internal waves," Geophys. Fluid Dyn. **3**, 225–264 (1972).
[2]C. Garrett and W. Munk, "Space-time scales of internal waves: A progress report," J. Geophys. Res. **80**, 291–297 (1975).
[3]J. L. Spiesberger and D. Green, "Statistical characterization of very low frequency communication channels at ocean basin-scales," Proceedings of the MTS-IEEE Oceans '06 Conference, Boston, MA (2006), pp. 1–6, Paper No. 060322-06.
[4]J. L. Spiesberger, "Comparison of measured and modeled temporal coherence of sound near 75 Hz and 3683 km in the Pacific Ocean," J. Acoust. Soc. Am. **124**, 2805–2811 (2008).
[5]J. L. Spiesberger, F. Tappert, and A. R. Jacobson, "Blind prediction of broadband coherence time at basin-scales," J. Acoust. Soc. Am. **114**, 3147–3154 (2003).
[6]J. L. Spiesberger, "Numerical prediction of coherent integration time at 75 Hz, 0.03 temporal resolution at 3250 km," Proceedings of the MTS-IEEE Oceans '06 Conference, Boston, MA (2006), pp. 1–4, Paper No. 060323-02.
[7]M. Vera and M. Dzieciuch, "Horizontal coherence in the NPAL experiment," J. Acoust. Soc. Am. **115**, 2617 (2004).
[8]V. E. Ostashev, A. G. Voronovich, and the NPAL Group, "Spatial coherence of acoustic signals measured during the 1998–1999 North Pacific Acoustic Laboratory (NPAL) experiment," J. Acoust. Soc. Am. **116**, 2608–2609 (2004).
[9]R. K. Andrew, B. M. Howe, J. A. Mercer, and the NPAL Group, "Transverse horizontal spatial coherence of deep arrivals at megameter ranges," J. Acoust. Soc. Am. **117**, 1511–1526 (2005).
[10]A. G. Voronovich and V. E. Ostashev, "Horizontal refraction of acoustic signals retrieved from the North Pacific Acoustic Laboratory billboard array data," J. Acoust. Soc. Am. **117**, 1527–1537 (2005).
[11]T. Rago, C. S. Chiu, C. S. Collins, P. F. Worcester, and C. Castro, "Oceanographic data from Sur Ridge (36.3° N, 122.4° W) to Hoke Seamount (32,1° N, 126.9° W)," Technical Report No. NPS-OC-00-002, Naval Postgraduate School, Monterey, CA, 1999.
[12]S. K. Han, C. Collins, C. Miller, C. S. Chiu, and P. Worcester, "Mapping the regional variability of the California Current acoustically using a waveform inversion method," J. Acoust. Soc. Am., **107**, 2862 (2000).
[13]J. L. Spiesberger, "An updated perspective on basin-scale tomography," J. Acoust. Soc. Am. **109**, 1740–1742 (2001).
[14]V. A. Del Grosso, "New equation for the speed of sound in natural waters with comparisons to other equations," J. Acoust. Soc. Am. **56**, 1084–1091 (1974).
[15]S. Levitus, "Climatological atlas of the world ocean," NOAA Professional Paper 13 (U.S. Government Printing Office, Washington, DC, 1982).
[16]A. Ben-Menahem and S. J. Singh, *Seismic Waves and Sources* (Springer-Verlag, New York, 1981), p. 1108.
[17]M. A. Wolfson and J. L. Spiesberger, "Full wave simulation of the forward scattering of sound in a structured ocean: A comparison with observations," J. Acoust. Soc. Am. **106**, 1293–1306 (1999).
[18]G. Laske and G. Masters, "A global digital map of sediment thickness," EOS Trans. Am. Geophys. Union **78**, F483 (1997).
[19]National Geophysical Data Center, "5 minute gridded world elevations and bathymetry—A digital database," ETOPO5, Boulder, CO, 1987.
[20]Naval Oceanographic Office Data Model, Oceanographic and Atmospheric Master Library (OAML), "Digital bathymetric database variable resolution (DBDB-V)," version 5.1, April, 2006.
[21]F. Tappert, J. L. Spiesberger, and L. Boden, "New full-wave approximation for ocean acoustic travel time predictions," J. Acoust. Soc. Am. **97**, 2771–2782 (1995).
[22]L. M. Brekhovskikh and Y. Lysanov, *Fundamentals of Ocean Acoustics* (Springer-Verlag, New York, 1982).
[23]J. Spiesberger, "Regions that influence acoustic propagation in the sea at moderate frequencies, and the consequent departures from the ray-acoustic description," J. Acoust. Soc. Am. **120**, 1842–1850 (2006).
[24]J. L. Spiesberger, "Comparison of two and three spatial dimensional solutions of the wave equation at ocean-basin scales in the presence of internal waves," J. Comput. Acoust. **15**, 319–332 (2007).
[25]A. K. Morozov and J. A. Colosi, "Stochastic differential equation analysis for ocean acoustic energy scattering by internal waves," J. Acoust. Soc. Am. **119**, 3344 (2006).